Steerable diffraction limited line illumination system using deformable mirror

Koichi Taniguchi*[a], Dae Wook Kim†[b], Kei Shimura[a] and James H Burge[b]
[a]Hitachi High-Technologies Corporation, 882 Ichige, Hitachinaka-shi, Ibaraki 312-8504, Japan
[b]College of Optical Sciences, University of Arizona, Tucson, Arizona 85721, USA

ABSTRACT

Many scientific and industrial applications often require high performance optical systems utilizing spatially shaped illumination patterns of laser beams. Precisely shaped line illumination can be used for various line scanning systems or surface inspection devices. In order to achieve the highest resolution or superior signal to noise ratio limited by the fundamental theory, a diffraction limited illumination optical system (e.g. >0.8 Strehl ratio) gives the narrowest illumination line width determined by the system's NA (Numerical Aperture) value. For high precision and in-factory industrial applications, the Diffraction Limited Line Illumination (DLLI) needs to be controlled in three dimensional space rapidly as the target object under the illumination may not be always aligned with respect to the illumination system. A steerable DLLI system with three degrees of freedom (i.e. axial displacement, rotation, and tilt) is developed using an adaptive optics system. By electronically controlling the Zernike based surface shapes of the deformable mirror, the DLLI in free space is actively positioned and oriented with high accuracy. The geometrical optics based mathematical model to control the Zernike modes of the deformable mirror and the performance of a bench-top proof-of-concept system will be presented with experimental data and analysis results.

Keywords: Adaptive optics, deformable mirror, beam shaping and line illumination

1. INTRODUCTION

Various laser beam shaping techniques have been developed and applied to high-power laser modules[1,2] or microscopy systems[3-6]. They often employ optimization techniques such as simulated annealing[7], stochastic parallel gradient descent[8], or genetic algorithms[9] to obtain ideal or arbitrary square, hollow, and so on spot shapes[10]. Most of them usually target symmetric or low aspect ratio focused spots utilizing rotationally symmetric lenses or mirrors.

A well-defined sharp line illumination is required for some advanced industrial applications such as substrate inspection systems using 1-dimensional linear image sensors. As the system scans the sample, the linear illumination needs to maintain its focus and location following the sample's surface. It is critical to control the narrow illumination pattern accurately so that high resolution scanning and illumination efficiency are achieved.

For industrial applications, the high accuracy and adaptability of the system for various conditions are important to keep high yield and flexible capability for different cases. For instance, the sample under inspection may experience some piston and tip-tilt motions for various reasons (e.g. varying sample's surface) and the illumination system needs to accommodate for these variations.

A steerable diffraction limited line illumination (DLLI) system has been developed and built as a bench-top proof-of-concept model. A commercially available adaptive optics sub-system using deformable mirror and wavefront sensor has been employed to take the advantage of its robust and real-time wavefront control features. The nominal DLLI pattern is accomplished by focusing collimated beam through a cylindrical lens. The deformable mirror provides required wavefront deformations to steer the illumination pattern swiftly in space.

* taniguchi-koichi@naka.hitachi-hitec.com

† letter2dwk@hotmail.com

Laser Beam Shaping XIV, edited by Andrew Forbes, Todd E. Lizotte, Proc. of SPIE Vol. 8843, 88430A

The steerable illumination pattern can be controlled in 3-dimensional space with 3 degrees of freedom: i) piston along the optical axis, ii) rotation about the optical axis and iii) tilt about the center of the line. These three motions are depicted in Figure 1. The theoretical derivation for the steerable DLLI is presented in Section 2. The bench-top proof-of-concept system is introduced in Section 3 along with its as-built performance demonstrations. Section 4 summarizes the results.

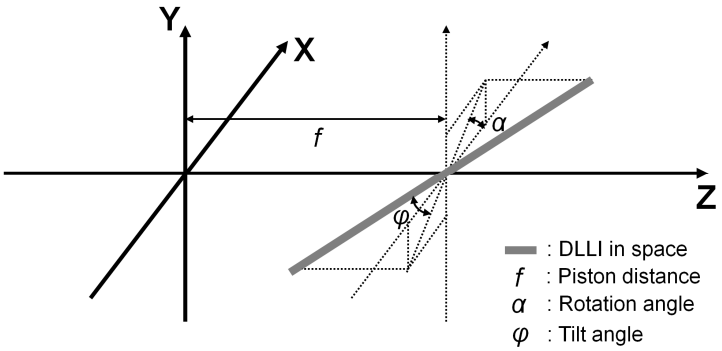

Figure 1. Three parameters defining the 3 degrees of freedom of DLLI (diffraction limited line illumination) in space

2. STEERABLE DIFFRACTION LIMITED LINE ILLUMINATION

2.1 Steerable DLLI System Overview

A schematic diagram showing the steerable DLLI system is shown in Figure 2. A collimated 635nm wavelength laser diode is used as a light source and an off-the-shelf cylindrical lens creates the nominal diffraction limited line illumination pattern in space. A deformable mirror is placed at the image conjugate location of the cylindrical lens (using an imaging lens) so that the wavefront deformation at the deformable mirror surface (i.e. steering wavefront) is directly added to the exiting wavefront from the cylindrical lens.

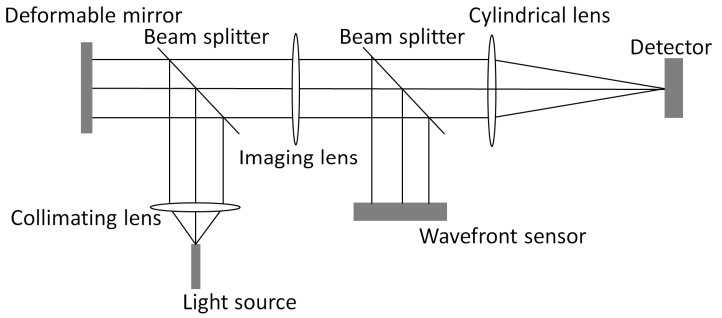

Figure 2. Schematic diagram showing the layout of the steerable DLLI system

2.2 Steering Wavefront

The wavefront control to steer the line illumination pattern is realized using the deformable mirror, which changes its mirror surface shape. The dynamic range and possible shapes are limited by the number of actuators, which define the available bending modes, and their stroke range. The target mirror deformation is often specified in terms of Zernike polynomials for a unit (radius = 1) circular pupil. For the proof-of-concept system in Section 3, the available bending modes were limited up to the 10^{th} Zernike polynomial Z_{10} as

$$Z_1 = 1 \qquad \text{(piston)} \tag{1}$$

$$Z_2 = x, \qquad Z_3 = y \qquad \text{(tip-tilt)} \tag{2}$$

$$Z_4 = 2x^2 + 2y^2 - 1 \qquad \text{(defocus)} \tag{3}$$

$$Z_5 = 2xy\,, \quad Z_6 = x^2 - y^2 \qquad \text{(astigmatism)} \tag{4}$$

$$Z_7 = 3x^2y + 3y^3 - 2y\,, \quad Z_8 = 3x^3 + 3xy^2 - 2x \qquad \text{(coma)} \tag{5}$$

$$Z_9 = 3x^2y - y^3\,, \quad Z_{10} = x^3 - 3xy^2 \qquad \text{(trefoil),} \tag{6}$$

where the x and y are the normalized coordinates within a unit circle ($-1<x<1$ and $-1<y<1$). These first 10 Zernike polynomials are shown in figure 3.

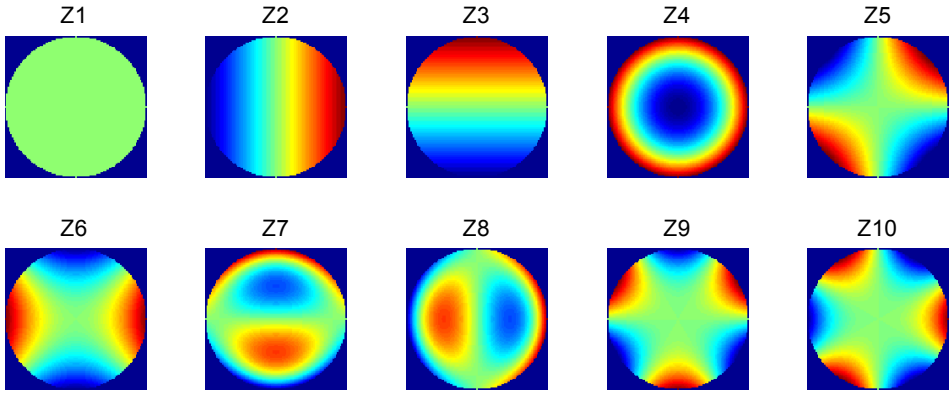

Figure 3. The first 10 Zernike polynomials within a unit (radius = 1) circle (Blue to Red: -1 to 1)

The steering wavefront can be expressed as the difference between the nominal wavefront W_0 exiting the cylindrical lens and the target wavefront W_t to achieve a newly positioned and oriented DLLI pattern. The ideal W_0 with focal length (of the cylindrical lens) f is given as

$$W_0 = \frac{r_p{}^2 \left(x\sin\alpha - y\cos\alpha\right)^2}{2f}, \tag{7}$$

where r_p is the pupil radius and α is the azimuthal angle of the DLLI in the x-y plane as shown in Figure 1.

The piston motion along the z-axis to translate the DLLI from f to a target f' sets the target wavefront as

$$W_{t\_piston} = \frac{r_p{}^2 \left(x\sin\alpha - y\cos\alpha\right)^2}{2f'}, \tag{8}$$

and the steering piston wavefront W_{s_piston} becomes

$$W_{s\_piston} = W_{t\_piston} - W_0 = \frac{r_p{}^2 \left(x\sin\alpha - y\cos\alpha\right)^2 \cdot (f - f')}{2f \cdot f'}. \tag{9}$$

The W_{s_piston} is decomposed using the Zernike polynomials as

$$W_{s\_piston} = C_4 Z_4 + C_5 Z_5 + C_6 Z_6, \tag{10}$$

where C_k represents the required k-th Zernike coefficient value. The coefficients are determined as

$$C_4 = \frac{r_p{}^2(f-f')}{8f\cdot f'},\quad C_5 = -\frac{r_p{}^2(f-f')}{2f\cdot f'}\sin\alpha\cdot\cos\alpha \text{ , and } C_6 = \frac{r_p{}^2(f-f')}{4f\cdot f'}\left(\sin^2\alpha-\cos^2\alpha\right). \quad (11)$$

The second steering motion, which rotates the DLLI about the z-axis to obtain a new azimuthal angle α', requires target wavefront

$$W_{t\_rotation} = \frac{r_p{}^2\left(x\sin\alpha'-y\cos\alpha'\right)^2}{2f}, \quad (12)$$

and in a similar way as equation (9) - (11), the steering rotation wavefront is determined as

$$\begin{aligned} W_{s\_rotation} &= W_{t\_rotation} - W_0 \\ &= \frac{r_p{}^2\left[x^2(\sin^2\alpha'-\sin^2\alpha)+y^2(\cos^2\alpha'-\cos^2\alpha)-2xy\left(\sin\alpha'\cos\alpha'-\sin\alpha\cos\alpha\right)\right]}{2f}, \\ &= C_5Z_5 + C_6Z_6 \end{aligned} \quad (13)$$

where

$$C_5 = -\frac{r_p{}^2\left(\sin 2\alpha'-\sin 2\alpha\right)}{4f} \quad \text{and} \quad C_6 = -\frac{r_p{}^2\left(\cos^2\alpha'-\cos^2\alpha\right)}{2f}. \quad (14)$$

The last steering wavefront, tilt about the center of the line in Figure 1, is expressed using the tilt angle φ as

$$W_{s\_tilt} = W_{t\_tilt} - W_0 = \frac{r_p{}^2\left(x\sin\alpha - y\cos\alpha\right)^2}{2(f + r_p\cdot\tan\varphi(x\sin(\alpha+90^\circ)-y\cos(\alpha+90^\circ)))} - \frac{r_p{}^2\left(x\sin\alpha - y\cos\alpha\right)^2}{2f}. \quad (15)$$

Unlike the other two motions, W_{s_tilt} cannot be fully decomposed using the first 10 Zernike terms, so that the limited (or approximated) Zernike representation in equation (16) was used to drive the deformable mirror shapes.

$$W_{s\_tilt} \approx C_2Z_2 + C_3Z_3 + C_7Z_7 + C_8Z_8 + C_9Z_9 + C_{10}Z_{10}, \quad (16)$$

where the Zernike coefficients are determined as

$$\begin{aligned} C_2 &= -\frac{r_p{}^3\cdot\tan\varphi}{12f^2}\left(\cos\alpha\sin^2\alpha+\cos^3\alpha\right), \quad C_3 = \frac{r_p{}^3\cdot\tan\varphi}{12f^2}\left(-\sin\alpha\cos^2\alpha-\sin^3\alpha\right), \\ C_7 &= \frac{r_p{}^3\cdot\tan\varphi}{24f^2}\left(-\sin\alpha\cos^2\alpha-\sin^3\alpha\right), \quad C_8 = -\frac{r_p{}^3\cdot\tan\varphi}{24f^2}\left(\cos\alpha\sin^2\alpha+\cos^3\alpha\right), \\ C_9 &= \frac{r_p{}^3\cdot\tan\varphi}{8f^2}\left(3\sin\alpha\cos^2\alpha-\sin^3\alpha\right) \text{ and } C_{10} = -\frac{r_p{}^3\cdot\tan\varphi}{8f^2}\left(3\cos\alpha\sin^2\alpha-\cos^3\alpha\right). \end{aligned} \quad (17)$$

3. BENCH-TOP STEERABLE DLLI SYSTEM

3.1 Proof-of-Concept Steerable DLLI System

A proof-of-concept steerable DLLI system was built using commercially available off-the-shelf components and adaptive optics sub-systems. An f/10 cylindrical lens with a focal length of 50mm was used as the main lens generating the nominal DLLI pattern. The overall configuration of the bench-top steerable DLLI system is shown in Figure 4.

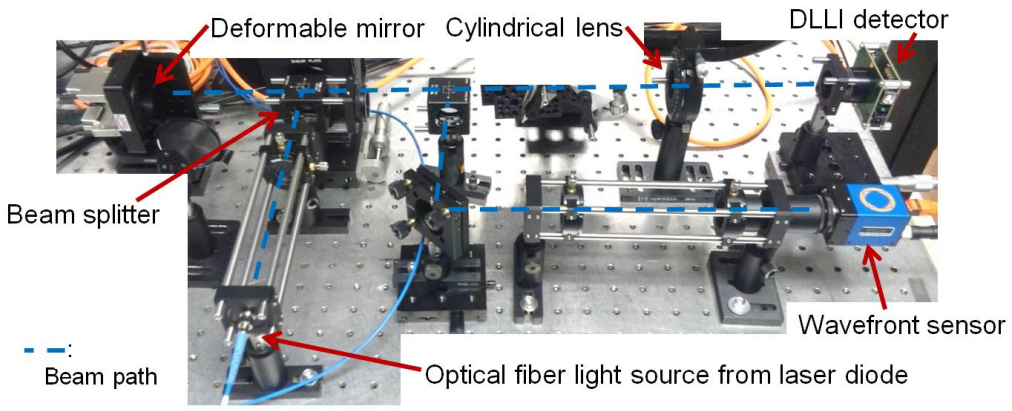

Figure 4. Bench-top proof-of-concept steerable DLLI system with the CMOS detector to measure the DLLI pattern

The ALPAO™ adaptive optics sub-systems including a deformable mirror (with 52 actuators over 15mm diameter circular area) and a Shack-Hartmann type OPTCRAFT™ wavefront sensor (with 37 by 28 lenslet array) were re-configured and used for the bench-top system. The deformable mirror was driven by a Matlab-based control software based on the steering wavefront calculations described in Section 2. The wavefront sensor was used to provide a feedback to the deformable mirror in order to achieve the target steering wavefront. The total response time of the active control system was ~20msec allowing real-time DLLI steering. Finally, the line illumination in space was measured using a CMOS detector (2.2μm pixel width) mounted on a tip-tilt and translation stage to evaluate the quality of DLLI and the performance of the overall system. The main components of the bench-top system are listed in Table 1.

Table 1. Main components' specification for the steerable DLLI system

Components	Specification	Manufacturer
Deformable mirror	52 actuators over 15mm diameter area (3μm inter actuator stroke range)	ALPAO™
Wavefront sensor	Shack-Hartmann with 37 by 28 lenslet array (6μrad angular sensitivity)	OPTOCRAFT™
Detector	CMOS with 2592 by 1944 pixels (2.2μm pixel width)	Lumenera® Corporation
Cylindrical lens	f/10 (focal length: 50mm)	Thorlabs™
Light source	635nm wavelength laser diode	Thorlabs™

3.2 Diffraction Limited Line Illumination

The line width and Strehl ratio of the line illumination was measured to verify the diffraction limited system. From the f/# of the cylindrical lens and the laser wavelength (λ=0.635μm) in Table 1, the ideal line width δ can be approximated as

$$\delta \approx 2.44\lambda \cdot f/\# = 2.44 \cdot 0.635 \cdot 10 = 15.494\,\mu m \ . \tag{18}$$

The average line width of the measured DLLI profiles was ~16-17μm which was close to the ideal diffraction limited case in Equation (18). A typical line illumination profile is presented in figure 5. Also, the measured Strehl ratio (1 for a perfect system) was >~0.8 in average.

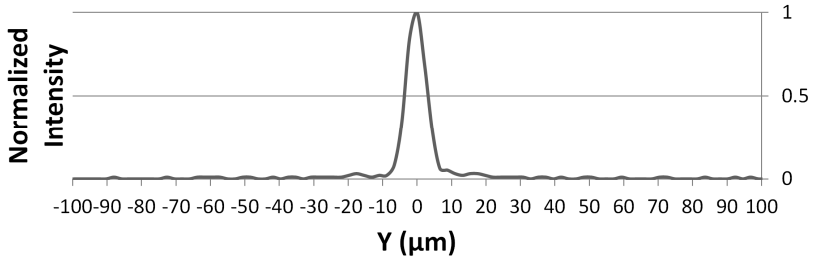

Figure 5. Normalized intensity profile of a DLLI across the line illumination pattern

3.3 Performance of the Steerable DLLI System

The steering range and linearity of the steerable DLLI system was tested and measured. The piston and rotation range was mainly limited by the deformable mirror's stroke range and shape accuracy. The effective steering range criterion was set as the range where the DLLI's average Strehl ratio is >0.8. The bench-top system achieved the steering ranges of +/- 3mm piston, +/- 2˚rotation, and +/-25˚ tilt motion. As an example, two DLLI images before and after a rotation are shown in Figure 6.

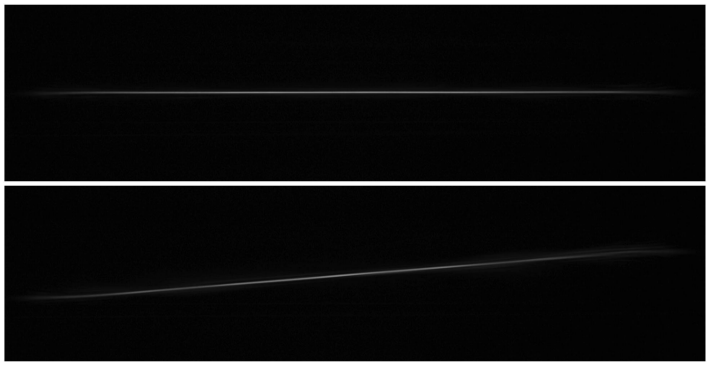

Figure 6. DLLI rotation measured by CMOS detector: before (top) and after (bottom) the rotation (Note: Both images are stretched in vertical direction to magnify the motion.)

The measured effective steering ranges and the linearity of the as-built steerable DLLI system show in Figure 4 are presented in Table 2.

Table 2. Effective steering ranges and the linearity of the as-built steerable DLLI system

Steering motion	Steering range	Linearity [q]
Piston	+/- 3mm	0.1 mm
Rotation	+/- 2˚	0.02˚
Tilt	+/- 25˚	1.2˚

[q] Standard deviation from the linear fit over the steering range

4. CONCLUSION

The proof-of-concept steerable DLLI system has been successfully built and its performance was demonstrated. The measured steering range and the linearity of each motion's control showed good performance without any fine tuning of the system. Further developments of the system and detailed investigation to characterize and calibrate the steering motion will be conducted. Also, utilizing more Zernike terms with larger dynamic range will be available using an upgraded deformable mirror system in the future.

REFERENCES

[1] S. W. Bahk, E. Fess, B. E. Kruschwitz and J. D. Zuegel, "A high-resolution, adaptive beam-shaping system for high-power lasers,"Opt. Express 18, 9151-9163 (2010).

[2] P. Yang, Y. Ning, X. Lei, B. Xu, X. Li, L. Dong, H. Yan, W. Liu, W. Jiang, L. Liu, C. Wang, X. Liang and X. Tang, "Enhancement of the beam quality of non-uniform output slab laser amplifier with a 39 actuator rectangular piezoelectric deformable mirror," Opt. Express, 18, 7121-7130 (2010).

[3] I. Izeddin, M. E. Beheiry, J. Andilla, D. Ciepielewski, X. Darzacq and M. Dahan, "PSF shaping using adaptive optics for three dimensional single-molecule super-resolution imaging and tracking," Opt. Express, 20, 4957-4967 (2012).

[4] M. Shaw, S. Hall, S. Knox, R. Stevens and C. Paterson, "Characterization of deformable mirrors for spherical aberration correction in optical sectioning microscopy," Opt. Express, 18, 6900-6913, (2010).

[5] W. Zou and S. A. Burns, "High-accuracy wavefront control for retinal imaging with Adaptive-Influence-Matrix Adaptive Optics," Opt. Express, 17, 20167-20177, (2009)

[6] O. Azucena, J. Crest, S. Kotadia, W. Sullivan, X. Tao, M. Reining, D. Gavel, S. Oliver and J. Kubby, "Adaptive optics wide-field microscopy using direct wavefront sensing," Opt. Letters, 36, 825-827, (2011)

[7] R. El-Agmy, H. Bulte, A. H. Greenaway and D. Reid, "Adaptive beam profile control using a simulated annealing algorithm," Opt. Express, 13, 6085-6091 (2005).

[8] H. Yang, Y. Liu, X. Li and X. Bi, "Technique of adaptive laser beam shaping based on stochastic parallel gradient descent,", Proc. SPIE, 7282, 72821W-1-72821W-6, (2009).

[9] P. Yang, Y. Liu, W. Yang, M. Ao, B. Xu and W. Jiang, "Adaptive Laser Beam Shaping Using a Genetic Algorithm," Proc. IEEE, 2906-2910 (2007)

[10] H. Ma, Q. Zhou, X. Xu, S. Du and Z. Liu, "Full-field unsymmetrical beam shaping for decreasing and homogenizing the thermal deformation of optical element in a beam control system," Opt. Express, 19, A1037-A1050, (2011).